Extreme motion and response statistics for survival of the M4 wave energy converter

H. Santo[a,*], P. H. Taylor[a], E. C. Moreno[b], R. Eatock Taylor[a], P. Stansby[b], L. Sun[c], J. Zang[c]

[a] *Department of Engineering Science, University of Oxford, Oxford OX1 3PJ, UK*
[b] *School of Mechanical, Aerospace and Civil Engineering, University of Manchester, Manchester M13 9PL, UK*
[c] *WEIR Research Unit, Department of Architecture and Civil Engineering, University of Bath, Bath BA2 7AY, UK*

Abstract

This paper presents linear analysis on extreme response statistics of the M4 wave energy converter in severe sea-states. A range of focussed wave groups were tested on a scaled M4 model without power take-off, which reveal the predominantly linear response structure in hinge angle and weakly nonlinear response for bending moment. There are complex and violent free-surface effects on the M4 model during the excitation period driven by the main wave group, which generally reduce the overall motion response. After the main group has moved away from the M4 model, the decaying response in the free-vibration phase decays at a rate very close to that predicted by simple linear radiation damping. With an experimentally and numerically derived response amplitude operator (RAO), we perform an extreme response statistics analysis for the central hinge angle of the machine at Orkney using wave data from the NORA10 hindcast from $1958 - 2011$. For storms with spectral peak wave periods longer than the machine RAO peak period, the machine response is controlled by the steepness of the sea-state rather than the wave height. Thus, the machine responds very similarly under the most extreme sea-states, providing an upper bound for the most probable maximum response. Four different assumptions on the sea-state are investigated: unimodal frequency distribution (total sea) with both unidirectional and directional spreading, and bimodal frequency distribution (total sea split into wind sea and swell) with directional spreading in both the same and different mean directions. There is a reduction in the extreme response of the machine when considering directionally spread waves compared to unidirectional. However, the reduction is only marginal when considering bimodal to unimodal frequency distribution with the

*Corresponding author
Email address: harrif.santo@eng.ox.ac.uk (H. Santo)

same directional spreading. Using a failure criterion derived from the present geometry of the M4 model and based on self-collision, the response statistics indicate that the slow drift yaw motion of the machine when considering lack of alignment in spread seas is an unimportant parameter for survivability. Finally, the effects of weakly nonlinearity in the response are discussed, nevertheless the response is remarkably linear in overall. The statistical methodology presented here is also potentially relevant to other wave energy converters in similar locations.
Keywords: M4 wave energy converter, extreme response, survivability, NewWave, focussed wave group

1. Introduction

Extreme response statistics for wave energy converters are key in determining the possibility of the survival of the device under extreme sea conditions. Previous studies have looked at the effects of extreme responses on the mooring lines, but few studies have concerned the extreme response of the device itself, e.g. see Parmeggiani et al. (2011); Muliawan et al. (2013a,b); Ambühl et al. (2014).

Previous work on the M4 wave energy converter has looked at the design and performance of the M4 machine in laboratory-scale experiments (Stansby et al., 2015a,b), and hydrodynamic-structural modelling with the power take-off modelled as a linear damper (Eatock Taylor et al., 2016). Using the same hindcast data, previous work has also looked at the decadal variability of practical mean wave power produced by the M4 machine at locations in the North-East Atlantic and North Sea, together with correlation with the NAO and other atmospheric modes (Santo et al., 2016a). Analysis on the wave climate alone using high quality NORA10 wave hindcast data has also been conducted to assess the decadal variability of the ocean wave power resource (Santo et al., 2015) and the 1 in 100 year extreme wave heights (Santo et al., 2016b), as well as their correlations to the NAO and other atmospheric modes.

The aim of this paper is to present study of extreme response statistics for the M4 wave energy converter. The focus is on the extreme responses, rather than power generated, hence only the cases without power take-off are considered, assuming the M4 machine power take-off is not operating under survivability (or extreme) conditions. We first describe experiments using focussed wave groups on a scaled M4 model in a wave tank. Focussed wave groups are used as a model for the average shape of extreme waves in a given sea-state, since regular waves are not representative

of an extreme wave, and random wave testing is time-consuming and the results are to some extent contaminated with wave reflections. We demonstrate that the device response is close to linear in hinge angle, with weak nonlinearity appearing in the bending moment in one of the beams in the machine. Thus, subsequent linear analysis on extreme response is justified. From the experimental results we obtain the machine response amplitude operator (RAO), which we combine with the numerically estimated RAO from the linear wave-diffraction code DIFFRACT. We perform NewWave-type response statistics calculations to obtain the most probable extreme response of the machine in any sea-state. We then conduct extreme response statistics based on 54 years using the same NORA10 wave hindcast data at Orkney from $1958 - 2011$, which is available for every 3 hours sea-state. The effects of nonlinearity due to large motions are discussed. We note that even though the focus is on the M4 machine, the statistical methodology presented in this paper is potentially relevant to other wave energy converters.

2. Experimental data and analysis

Experiments on focussed wave groups were conducted in the COAST (Coastal, Ocean and Sediment Transport) laboratory of Plymouth University. The wave tank is 35 m long and 15.5 m wide. It has an adjustable basin floor, which was set at 1 m water depth for the experiments reported here. The wave paddle array is a set of the Edinburgh Design (EDL) bottom hinged paddles, and linear wave generation was used. The far end of the wave tank is equipped with 1:20 sloping ramp covered with a porous material acting as a passive absorber. The layout (side view) of the experimental setup together with the M4 machine is shown in Figure 1. The M4 machine is a three-float system, each float with a circular cross-section when viewed from above. Float 1 and 2 are rigidly connected, and the larger float 3 is connected to the mid float by an articulated joint (or hinge, where the beam from float 3 is joined to float 2). The machine generates power through the relative angular motion of this articulated joint between these two floats. The M4 machine is connected to an elastic mooring line through a floating buoy to prevent the model from drifting.

A wave group is made to focus when a set of Fourier components are aligned in phase at a single position in space and time (constructive interference). Fetch-limited JONSWAP spectrum with $\gamma = 3.3$ for the peak enhancement factor was used, and the input spectrum was truncated at 2 Hz. Two sets of wave groups were considered: linear crest amplitude at focus (A_c) of 0.0245 and 0.08 m. For each A_c, there are six different peak spectral periods (T_p) of 0.8, 1.0, 1.1, 1.2,

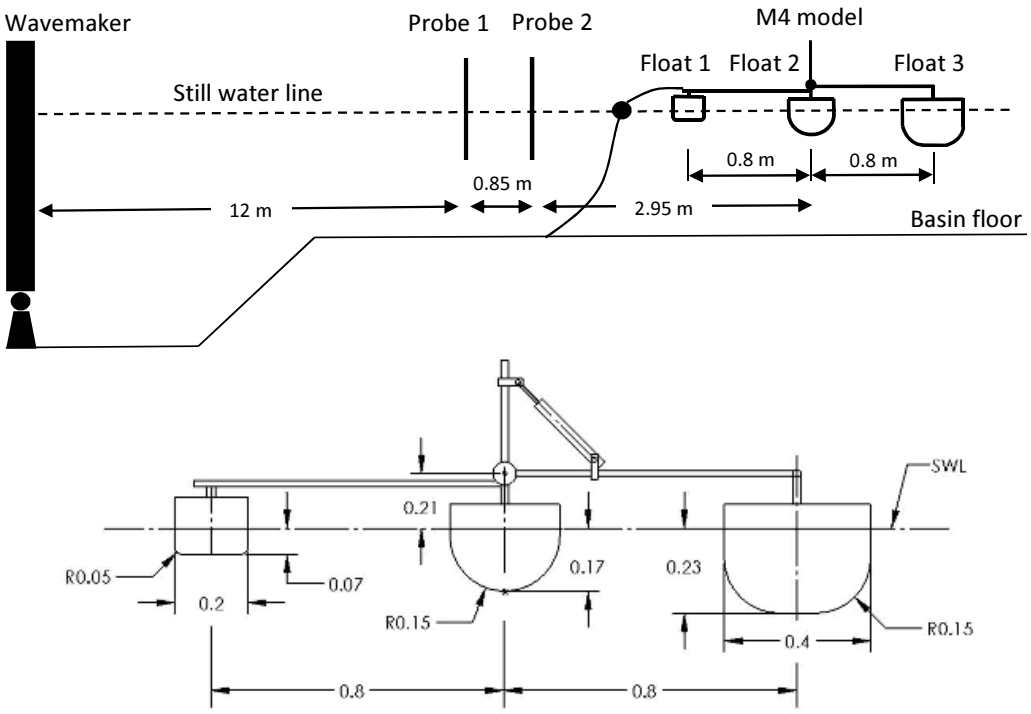

Figure 1: Top figure shows the layout (side view) of the experimental setup with the lab-scale M4 model (not to scale). Bottom figure show the dimensions (in metre) of the M4 model.

1.4, and 1.6 sec. T_p of 1.2 sec is taken as the base case for each A_c, as the M4 machine responded most vigorously close to this peak period. For each test, several parameters were measured in time: hinge angle response (°), positions of the hinge and top of the float 3 (processed using a Qualysis motion tracking system, the small white reflectors are visible in Figure 3), surface elevations at two wave probes upstream of the M4 machine, bending moment at a point in the beam close to float 2, and mooring force. The sampling frequency for surface elevation is 128 Hz, while for the other signals 200 Hz. The duration for each test is about 120 sec.

2.1. Measured response in hinge angle and bending moment

Examples of the measured data are presented in Figure 2 for two wave amplitudes both with $T_p = 1.2$ sec. The figure shows the surface elevation obtained from probe 1 upstream of the M4 machine (see Figure 1), the hinge angle response (°), and the bending moment between float 1 and 2 (see Figure 1). From the plots of the surface elevation - time history, it is clear that the dispersive

wave group will evolve in time and space between 70 - 80 sec before reaching the model. On the basis of linear wave theory, the wave group should focus at the location of the model (assumed to be at the centre of float 2, which is 3.8 m downstream of probe 1), with the resultant temporal shape symmetric in time around the largest peak crest (not shown). Between 85 - 95 sec at the upstream wave probe, one can see (linear) scattered waves from buoy and the model, both interacting with the (second order double frequency) error waves which arrived later after the main dispersive wave group has gone. From the hinge angle response - time history, one can see a fast build-up of the response as the wave group hits the model, and after the group has passed through the model, the model was undergoing prolonged free vibration. Similar behaviour is observed for the bending moment - time history. Qualitatively, the temporal shape of the response in hinge angle is very close to symmetric vertically, suggesting that the hinge angle response is predominantly linear. The temporal shape of the bending moment is however more vertically asymmetric, hence more nonlinear.

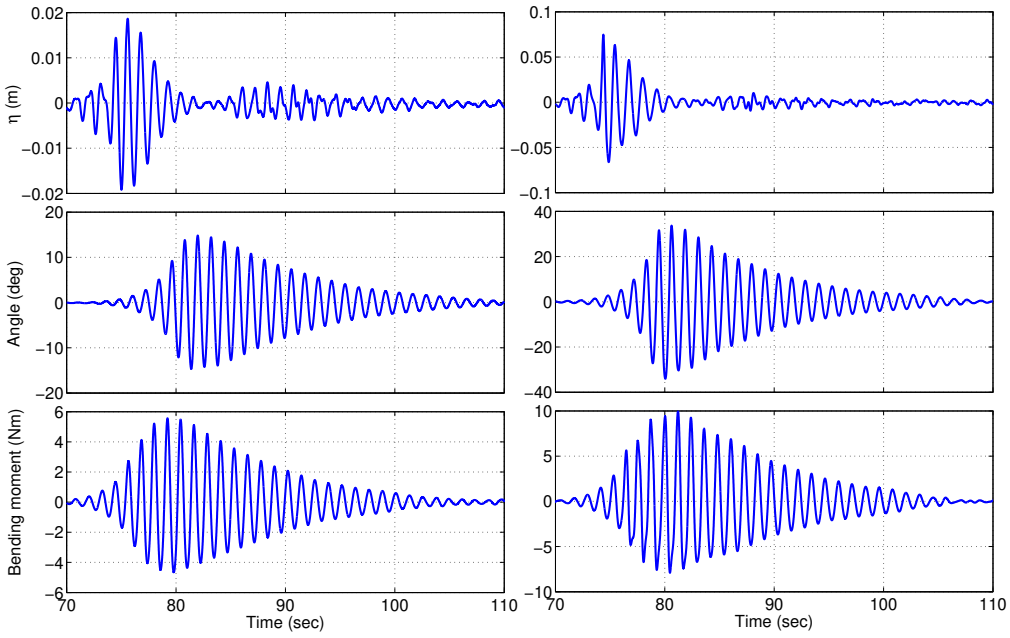

Figure 2: Examples of the measured data for $A_c = 0.0245$ m (left panel) and 0.08 m (right panel), all for $T_p = 1.2$ sec. Top row shows the surface elevation - time history from probe 1 upstream of the M4 machine, see Figure 1. Middle row shows the hinge angle response - time history. Bottom row shows the bending moment - time history between float 1 and 2, see Figure 1.

A more detailed localised behaviour is presented in Figure 3 which show series of snapshots of the M4 machine for the large amplitude wave group of $A_c = 0.08$ m and $T_p = 1.2$ sec. The top figure shows the instant when float 1 and (red) buoy were being submerged (dunked) as the wave group arrived, the direction of wave motion is from right to left. The middle figure shows the instant when float 2 was being dunked as the largest crest in the wave group arrived at the focus location. The bottom figure shows the instant of the maximum hinge angle response (here with almost self-collision between the centre float and the freely pivoting beam), during the free vibration as the wave group passed through the model. At this instant, floats 1 and 3 were almost dunked and the (red) buoy was completely submerged below the water surface, demonstrating violent conditions for the M4 machine during a representation of an extreme event. Throughout some of the large wave group events, there were complicated localised events of floats being dunked and layers of green water on top of the floats and beams connecting the floats, which altogether have the effect of reducing the machine response. Remarkably, the measured hinge angle response is nevertheless predominantly linear. For the lower amplitude wave group of $A_c = 0.0245$ m, the top of all three floats remained dry throughout the event.

All cases were tested with a wave group focussed at the location of the M4 machine (crest focussed), no inverted wave group tests (trough focussed, by shifting each phase of wave component by π) were done. Hence, frequency filtering is required to separate the harmonics contribution, which works reasonably well because both the surface elevation and response spectra are sufficiently narrow-banded, see Figure 4. The harmonic decomposition of each of measured time history is also presented in the same figure. Qualitatively, the structure of the signals for the surface elevation and hinge angle is dominated by the linear component, and as observed earlier, the structure for the bending moment contains slightly more nonlinearity.

Here the observed nonlinear effects are investigated further. If the motion nonlinearity is simply scaled according to Stokes perturbation theory, the nonlinear higher order harmonics components simply scale with and are bound to the linear component. If however the effect of local nonlinear effects such as quadratic viscous damping is significant, any contribution from this Morison-type of drag term would produce linear and triple frequency components, i.e. $v^2 \cos\Phi |\cos\Phi| \sim (8/3\pi)v^2(\cos\Phi + 1/5 v^2 \cos 3\Phi)$, as well as the simpler nonlinear contributions following the mathematical structure of Stokes perturbation theory for nonlinear potential flow. It will be shown that there is no observed any significant contribution from such a Morison drag term.

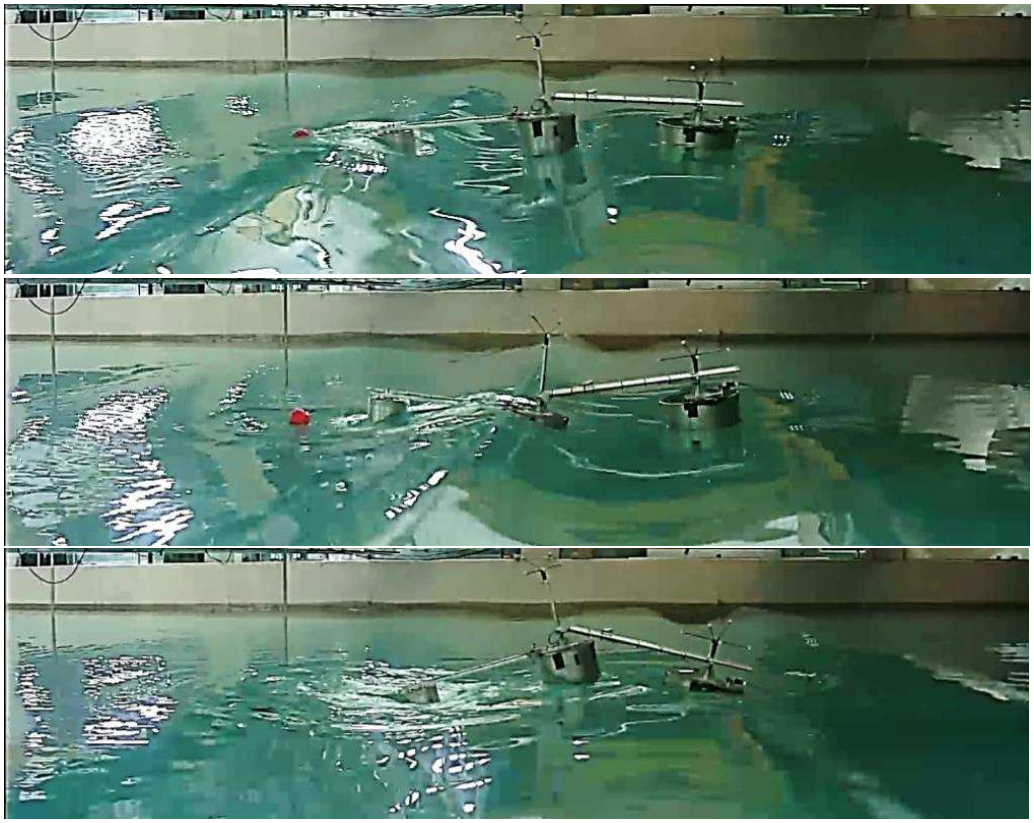

Figure 3: Series of snapshots of the M4 machine for the focussed wave group of $A_c = 0.08$ m and $T_p = 1.2$ sec. Top figure shows float 1 and (red) buoy being dunked as the wave group was arriving. Middle figure shows float 2 being dunked when the wave group was focussed in space and time. Bottom figure shows the maximum hinge angle (almost self-collision) during free vibration as the wave group passed through the model, where floats 1 and 3 were almost dunked and (red) buoy completely submerged from the water surface. The two vertical bars at the right side of each figure are the upstream wave probes. The wave group travels from right to left.

For a narrow-banded process, it should be possible to approximate the double frequency and triple frequency contributions in terms of the linear component, see for example Walker et al. (2005). For a given linear signal $\eta_L = a(t)\cos\Phi(t)$ where $a(t)$ is the slowly varying amplitude of the signal in time and $\Phi(t)$ is the phase of the signal, the Hilbert transform of the linear record (which introduces $\pi/2$ phase shift into the signal) can be written as $\eta_{LH} = a(t)\sin\Phi(t)$. Thus, the double frequency contribution can be approximated in terms of the combination of the linear and

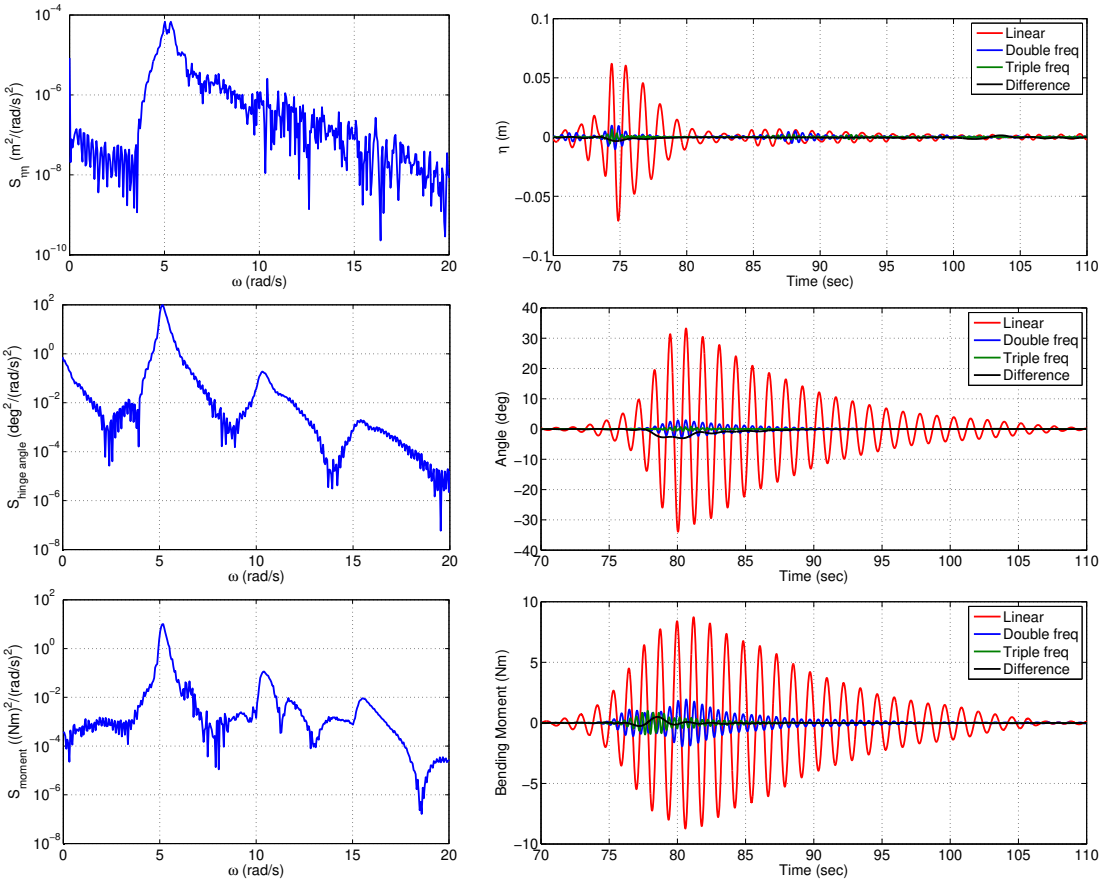

Figure 4: Left panel: Power spectra of the surface elevation (top), hinge angle (middle) and bending moment (bottom) for $A_c = 0.08$ m and $T_p = 1.2$ sec. Right panel: Harmonic structure of the surface elevation (top), hinge angle (middle) and bending moment (bottom) for the same case. The linear components are in red, double frequency components in blue, difference components in black, and triple frequency components in green. The total signal for each is shown in Figure 2.

its Hilbert transform, with appropriate vertical scaling, as:

$$\eta_2 = a^2 \cos 2\Phi = \eta_L^2 - \eta_{LH}^2, \tag{1}$$

and the third order contribution as:

$$\eta_3 = a^3 \cos 3\Phi = \eta_L(\eta_L^2 - 3\eta_{LH}^2). \tag{2}$$

Thus, to investigate whether Stokes scaling is valid or whether there is viscous damping in the measured responses, we fit η_2 and η_3 to the double frequency and triple frequency contributions

of the hinge angle and bending moment signals. This is shown in Figure 5 for both A_c values and $T_p = 1.2$ sec. The fits are performed for the portion of the response signals after the wave group has passed by, i.e. from 80 sec. As might be expected, the fit to the hinge angle is good for the double frequency component, however the triple frequency signal is more complex as the wave group passes by and of much smaller magnitude compared to the linear component, hence the fit is not shown. The fit to the bending moment is reasonable for the double frequency component, with some mismatch before 80 sec (before the main wave group arrives). For the fit at triple frequency component, the mismatch is more pronounced before 80 sec, and the fit is subsequently better. The mismatch before 80 sec could be due to quadratic viscous damping at triple frequency component, and/or the fact that bending moment is a result of double differentiation in time of a displacement, which amplifies high frequency nonlinear contributions noise. Hence, in general the harmonic structure of the bending moment is more complex than that of the hinge angle.

From 80 sec onwards, the synthetic double and triple frequency components, derived from the linear signal, fit the measured signals well, both in terms of phase and also the decay of the amplitude of free vibration over time. Also of importance is that this decay is a simple exponential in time, and has the same rate for all groups, large and small, and with various peak wave periods – it corresponds almost exactly to simple linear damped free vibration of the M4 machine in otherwise still water, and double that decay rate for the second order double frequency component, and triple that for the third order triple frequency component. We obtain as a third order / harmonic approximate fit:

$$\begin{aligned} \phi &= \phi_L + 0.00215(\phi_L^2 - \phi_{LH}^2) + (\sim 10^{-5})\phi_L(\phi_L^2 - 3\phi_{LH}^2), \\ BM &= BM_L + \frac{0.0165}{\rho g L^4}(BM_L^2 - BM_{LH}^2) + \frac{0.0004}{(\rho g L^4)^2} BM_L(BM_L^2 - 3BM_{LH}^2), \end{aligned}$$

for all wave groups and for times > 80 sec, where ρ is the water density, and L is the beam length (0.8 m). This approximation to the hinge motion (ϕ) and bending moment (BM) fits well. It should be noted that there is a phase shift (~ 2.5 rad) required to fit the triple frequency component of the bending moment, while no phase shift is required to fit the double frequency component of the bending moment, and the double and triple frequency components of the hinge angle.

The reasonably good agreement using the approximation based on the linear component and its Hilbert transform to the higher order harmonics demonstrates that much of the nonlinearity observed in the measured data is of Stokes perturbation-type (simply bound to the linear component).

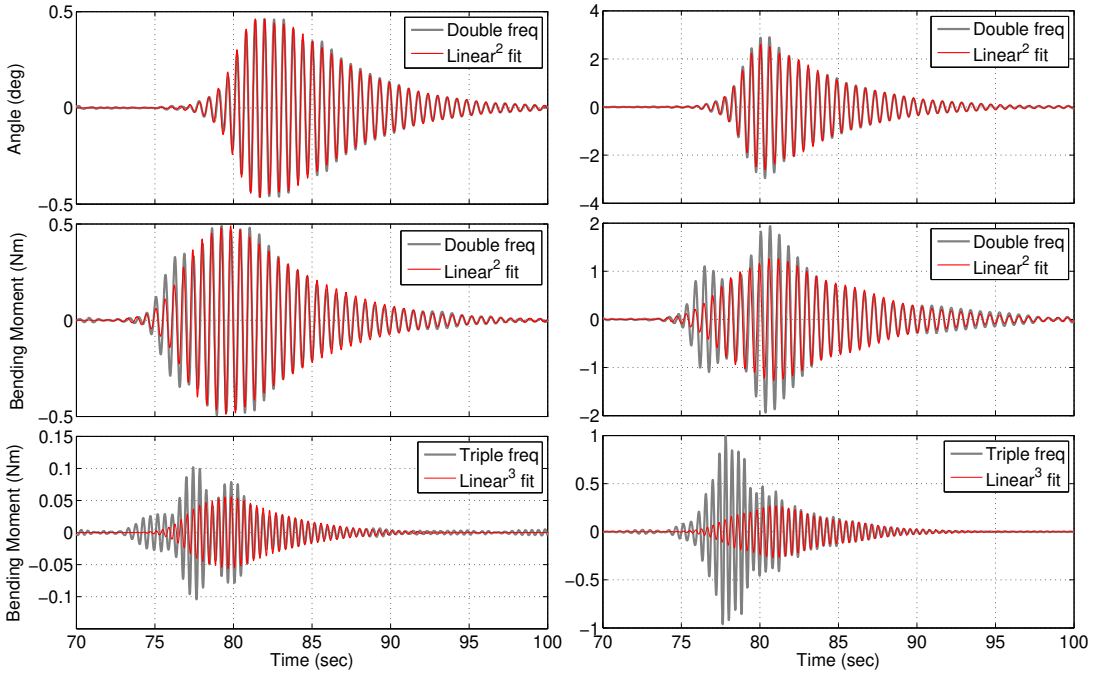

Figure 5: Comparison of the higher harmonics signals (thick black line) and the fit using linear signal approximations (thin red line) for $A_c = 0.0245$ m (left panel) and 0.08 m (right panel), all for $T_p = 1.2$ sec. First row shows shape comparison of double frequency component in terms of hinge angle. Second and third row show shape comparison of double and triple frequency component in terms of bending moment.

Arguably, there is more nonlinearity observed for the higher A_c case, which is not fitted quite so well by the approximation. It is worth mentioning that, apart from the possible contribution from the viscous damping, there were complicated localised events of floats being dunked and trapped green water which must contribute nonlinearity, see Figure 3. The overall fit at the third order component is less satisfactory, but the magnitude is much smaller compared to the linear component and again the fit is good for the later free vibration phase. Hence, it is reasonable to assume the M4 machine response in both hinge angle and bending moment is predominantly linear, with small nonlinear contributions scaling according to Stokes harmonics (weakly nonlinear). The effect of damping is shown to be relatively small, consistent with Eatock Taylor et al. (2016). We return to the value of the observed linear damping rate later.

2.2. The RAO

The response amplitude operator (RAO) describes the linear relationship between an input signal and the resultant response. Here the modulus of the RAO can be written as:

$$|RAO| = \sqrt{\frac{S_{response}}{S_{\eta\eta}}} \tag{3}$$

where $S_{\eta\eta}$ is the power spectrum of the surface elevation, and $S_{response}$ is the power spectrum of the hinge angle or the bending moment. For each wave group test, the RAO is obtained and averaged across all the cases in the complex form for two different A_c. It should be noted that the shape of the incident wave at probe 1 changes as it advances to the focus location. This is allowed for using linear deepwater dispersion theory. This is necessary to produce the correct phase information of the wave, and subsequently of the measured RAO. It is this linear crest amplitude at the focus location which defines A_c.

The experimentally derived RAOs are plotted as solid lines in Figure 6 after a 5-point frequency smoothing of the power spectra. The RAO curve is linear within the the most energetic frequency excitation range (from $\omega = 4 - 8$ rad/s), with some nonlinearity contaminating the curve to the left and right side of the peak. Two experimentally based RAOs are shown. These are very similar in shape; with the peak RAO for $A_c = 0.08$ m being smaller than that for $A_c = 0.0245$ m, presumably due to the effect of nonlinearity – local submergence of the floats, layers of green water, and viscous damping for very large relative motion, which generally reduces the overall machine motion.

Instead of simply linearising the experimental RAO for use in subsequent analysis, we choose to make use of the numerically estimated RAO using the wave-diffraction boundary element code DIFFRACT (Eatock Taylor and Chau, 1992; Sun et al., 2015). This is helpful because the variation of the RAO as a function of incident wave direction for the subsequent extreme response statistics can be derived numerically, where no experimental data is available. The DIFFRACT code is used to solve the linear diffraction, radiation and hydrodynamic interactions between each float of the M4 machine in a two-body model, with float 1 and 2 modelled as a single body with the appropriate hydrodynamic properties. The code runs in the frequency domain, and the resulting RAO is combined with the input wave components and summed across the finite range of linear frequencies. Each float is modelled with the same geometric and mass/inertia values as used in the experiments. The small red buoy visible in Figure 3 is not modelled in the simulation as its effect is assumed to be negligible, and the mooring line is also omitted. Being a linear model, the

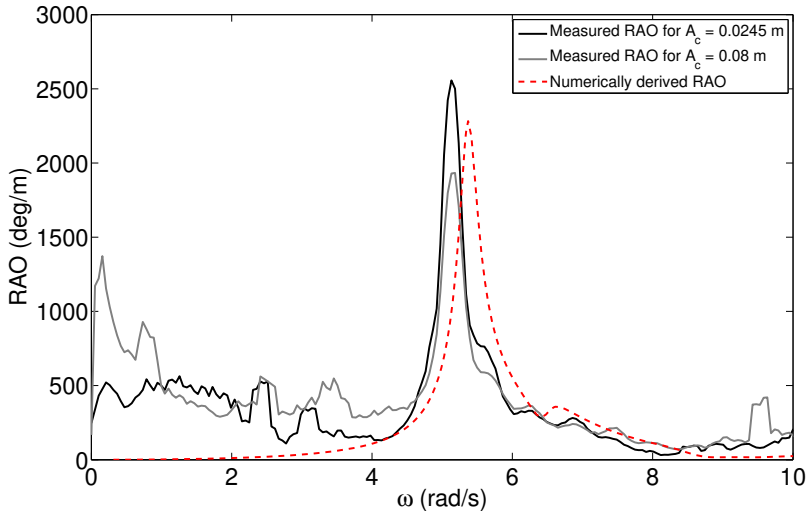

Figure 6: Comparison of the RAOs derived from wave group experiments with $A_c = 0.0245$ and 0.08 m (black and grey lines, respectively) and numerically derived RAO using linear potential diffraction solver DIFFRACT (dashed line).

only damping term that is present in the numerical simulation is the radiation damping, which can be predicted using DIFFRACT. In the actual experiments however, there is likely to be additional damping.

The numerically derived RAO is presented as the dashed line in Figure 6. Comparing the shape with the experimentally measured RAOs, the peak numerical RAO is slightly smaller than the RAO for the smaller A_c, and there is a small upwards shift in the peak frequency. Ideally, the numerical RAO should be higher than the measured ones, having no damping other than radiation damping in the simulation. We are unable to identify what causes the shift in both the peak frequency and the peak value. The shift could be due to advection effects, as the device is moving quite markedly (mostly in surge motion) as the focussed wave group arrives and the measurements are made relative to a fixed frame of reference. The shift could also be due to device mistuning in either experiments or numerical simulation, or a small misrepresentation of geometry and/or moment of inertia. It should be noted however that, if the numerical RAO is adjusted in both frequency and peak value to fit the measured RAO for the smaller A_c, the overall shape is very similar within the most energetic frequency excitation range (from $\omega = 4 - 8$ rad/s), and this now provides additional information on the shape of the low and high frequency tails of the RAO. With this regard, we

choose to use this modified numerical RAO for our subsequent analysis.

Figure 7 shows a comparison of the experimentally measured $|RAO|$ and phase shift for the M4 machine and the scaled versions of the DIFFRACT numerical results - essentially curve fits. Both the amplitude and phase match well. Interestingly, if the original numerical results are Froude scaled to shift the frequency of the peak of the RAO curve down by 5%, this increases the RAO peak value for angle by 10%: all equivalent to increasing the machine size by 10%. This achieves a very good fit to the experimentally determined RAO curve.

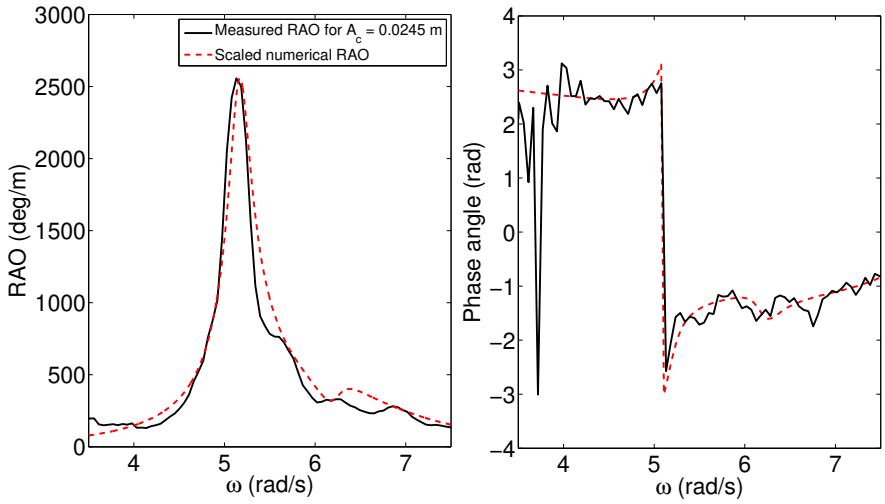

Figure 7: Comparison of the RAOs derived from wave group experiments with $A_c = 0.0245$ (solid line) and scaled RAO using DIFFRACT (dashed line) in terms of amplitude (left figure) and phase angle (right figure).

The variation of the RAO with respect to incident wave direction was obtained numerically with DIFFRACT and plotted in Figure 8, with the M4 machine aligned along the direction of wave propagation being taken as 0°. Along the peak frequency, the RAO is pretty flat within ±30° incident wave direction, beyond which there is a rapid fall off as the direction increases further. The variation with frequency is quite narrow-banded for each wave direction. For 0° wave direction, the shape of the RAO recovers to the modified RAO in Figure 7.

2.3. The damping behaviour

We now examine the behaviour of the free decay of the machine angular displacement after the wave group has passed by and the free-surface in the region of the model has returned to rest, apart from that induced by motion of the machine. From the RAO curve, we examine the peak value and

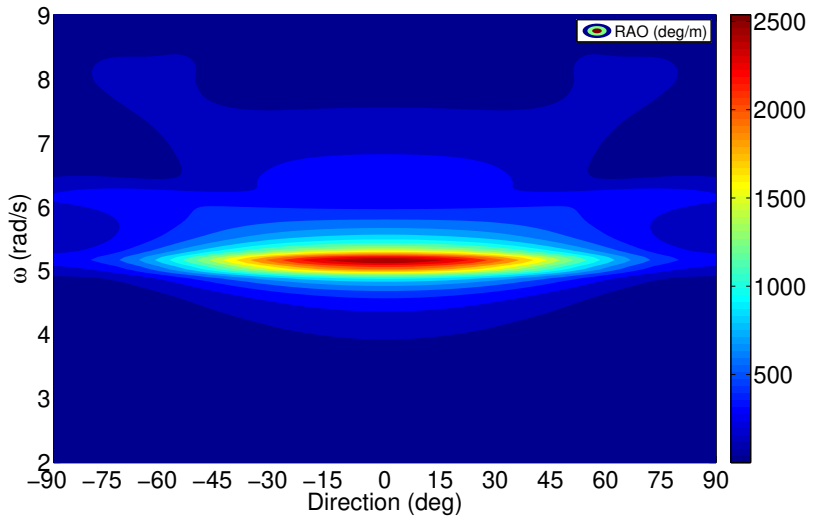

Figure 8: Presentation of the numerically derived 2D RAO as a function of frequency and incident wave direction.

the two half-power points where the value of the RAO is reduced to $1/\sqrt{2}\times$ peak. For simple linear systems (Newland, 2006, p. 72), the width of the resonant peak is related to the linear damping by $\Delta\omega/\omega_R \sim 2\zeta$, where ω_R is the resonant frequency, and ζ is the non-dimensional damping rate. For the small amplitude group RAO, this gives a numerical value of $\zeta \sim 0.025$. This damping is similar for both the physical experiment and the scaled DIFFRACT numerical result. This implies that only radiation damping is important during these wave group tests. Viscous effects seem to be small in comparison.

For weakly damped linear resonant systems, the free vibration amplitude decays as $\theta \sim \theta_0 \exp(-\zeta\omega_R t)$, where θ_0 is the initial amplitude. Hence, we can also estimate the appropriate value of damping from the experimentally measured motions after the wave group has moved away from the M4 model, a time we estimate as ~ 85 sec.

Figure 9 shows the envelopes of the hinge angle response of the M4 machine with time for all the wave group tests ($T_p = 0.8$, 1, 1.1, 1.2, 1.4 and 1.6 sec) for two amplitudes: $A_c = 0.0245$ m shown in black lines, and $A_c = 0.08$ m in grey lines. The envelopes are all multiplied by an exponential group term, $\exp[0.023\omega_R(t-85)]$. The red solid line is the average of the smaller amplitude response taken from $85 - 100$ sec. Clearly, the portions of all the envelopes for $t > 85$ sec are close to horizontal – showing that in <u>all</u> cases the decay of the free oscillations of the machine are close to linear with a damping value $\zeta \sim 0.023$. This value is only 8% lower than that estimated from the half-power

width of the RAO curve. For $T_p = 0.8$ sec, there is not enough excitation energy to drive the M4 machine for both amplitudes. For almost all cases, the amplitude for free-vibration phase is dependent on the size of the wave group, except for $T_p = 1.4$ sec, where presumably something odd happening to one of the floats.

On the same figure, the blue dashed line represents where the larger amplitude response envelope would have been if the whole process was linear (scaling the red solid line by the ratio of the large to small linear wave amplitudes at focus). Comparing the blue dashed line with the actual measured larger amplitude response envelope (grey lines) give an idea of how much response is lost by nonlinearity in the excitation phase. Linear scaling is always expected to be conservative, hence for almost all cases the dashed blue line is always above the red solid line. However, it is not clear why this is not the case for $T_p = 1$ sec, although there is admittedly different nonlinear contribution to the machine coupling to the response for each T_p. It should be noted however that all the design cases leading to failure have storm T_p close to or longer that the machine peak RAO period (~ 1.2 sec at lab scale), hence arguably only cases from $T_p = 1.1 - 1.6$ sec are more important and relevant for survivability.

Applying the same methodology to the envelopes of the linearised bending moment for all the wave group tests yields the same damping value $\zeta \sim 0.023$ for the decay during the free oscillations of the machine. In terms of the half-power points of the bending moment RAO, both measurement and numerical results give $\zeta \sim 0.0255$. This finding, consistent with the damping behaviour observed for the hinge angle response, further supports the observation that only radiation damping is important for these tests. We also observe similar odd behaviour for $T_p = 1$ and 1.4 sec in the envelopes of the linearised bending moment.

Overall and remarkably, in all cases this damping behaviour is simply linear, even starting from a rotation angle of close to 25°. We associate this damping with linear wave radiation outwards and generated by machine motion in otherwise still water. Even for a rotation angle of 25°, there seems to be little viscous damping – an observation supported by a heaving ring of eight similarly sized cylinders recently reported by Wolgamot et al. (2016) with oscillation periods close to 1 sec.

3. NewWave in response

Here we present a methodology to obtain the most probable maximum response of a wave energy converter in a realistic sea-state condition. For linear random waves with Gaussian surface elevation

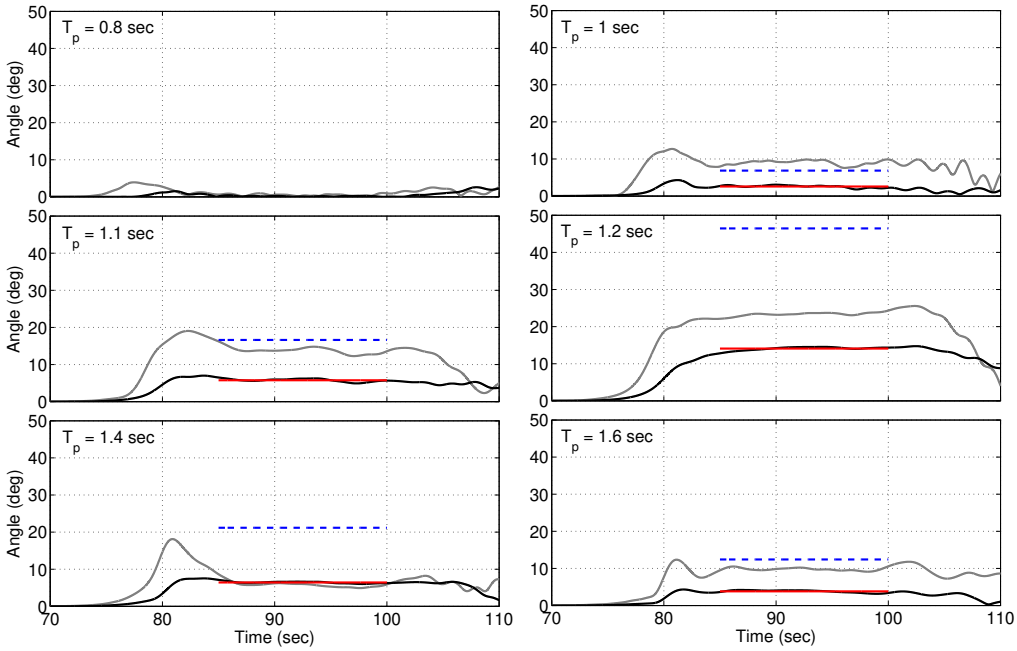

Figure 9: Envelopes of the hinge angle response of the M4 machine with time, which have been multiplied by $\exp[0.023\omega_R(t-85)]$, for all wave group tests and for two amplitudes: $A_c = 0.0245$ m shown in black lines, and $A_c = 0.08$ m in grey lines. Red solid line is the average of the smaller amplitude response taken from $85-100$ sec, while blue dashed line is the same response scaled up by the ratio of the large to small linear amplitudes at focus, over the same time interval.

statistics, the average shape of the largest wave in time tends to a scaled autocorrelation of the underlying wave spectrum (Lindgren, 1970; Boccotti, 1983), and this concept was brought into offshore engineering by Tromans et al. (1991), where it became known as NewWave. A comparison was made between the measured large linearised crests and equivalent predictions by the NewWave model for time series recorded offshore in the North Sea (Jonathan and Taylor, 1997) and in the Gulf of Mexico (Santo et al., 2013). The agreement was excellent, justifying the application of NewWave as a reasonable model for the linear part of large offshore wave crests.

This NewWave concept in wave crest statistics was further extended to the average shape of structural response (NewWave in response) by Grice et al. (2013), who looked at the resultant crest elevations and wave run-up on four-leg semi-submersible platform under focussed wave groups. Here we apply a similar NewWave in response methodology to the M4 machine in terms of hinge angle and bending moment, for a given sea-state.

For a stationary narrow-banded Gaussian random process, it can be assumed that the individual waves and machine responses follow a Rayleigh distribution in amplitude. In this application, it should be noted that the machine responses are dominated by the main resonant peak, so are considerably more narrow-banded than the incident wave field. The normalised probability density function for the amplitude can be written as:

$$p(\xi) = \xi \exp(-\xi^2/2), \tag{4}$$

where $\xi = \alpha/\sqrt{m_0}$ is the normalised amplitude, and m_0 is the total variance of the spectrum, $S(\omega_n)$, given by $m_0 = \sum_{n=0}^{\infty} S(\omega_n)\Delta\omega$. For a single wave or response, the probability of its amplitude being less than α is:

$$P(\xi) = \int_0^{\xi} p(\xi')d\xi' = 1 - \exp(-\xi^2/2). \tag{5}$$

Thus, for N statistically independent waves or responses, the probability that the amplitude α will be exceeded at least once is given by:

$$1 - P^N = 1 - \left[1 - \exp(-\xi^2/2)\right]^N. \tag{6}$$

The probability density of the largest value in N waves or responses can be derived from this, and the peak of the probability density function, which is the most probable extreme wave or response amplitude in N samples, can be approximated for large N as:

$$\alpha = \sqrt{(2m_0 \log N)}. \tag{7}$$

In general, N is obtained from the zero crossing period (T_z) of waves or responses in a 3 hour sea-state, with $T_z = \sqrt{m_0/m_2}$, and $m_2 = \sum_{n=0}^{\infty} \omega^2 S(\omega_n)\Delta\omega$. However, for the M4 machine we can simply take the period corresponding to the peak of the RAO curve.

By superposition of monochromatic deterministic plane waves, one can write an expression for the surface elevation for general wave motions as

$$\eta = \mathrm{Re}\left[\sum_n \sum_k A_{nk} \exp\left(i\omega_n t - \kappa_n x \cos\theta_k - \kappa_n y \sin\theta_k\right)\right] \tag{8}$$

where A_{nk} is a random variable compatible with wave directional spectrum, ω is the wave frequency, κ is the scalar wavenumber, θ is the angle of incidence relative to the x-axis. Similarly, the

expression for the response such as hinge angle (ϕ) can be obtained by convoluting A_{nk} with the two-dimensional RAO, or Z_{nk} say.

In terms of power spectra, the spectrum of response angle ϕ is expressed as:

$$S_{\phi\phi}(\omega_n) = S_{\eta\eta}(\omega_n) \sum_k |Z_{nk}^2(\omega_n, \theta_k)| H_{nk}(\omega_n, \theta_k) \Delta\theta \tag{9}$$

where $S_{\eta\eta}(\omega_n)$ is the power spectrum of surface elevation, and $H_{nk}(\omega_n, \theta_k)$ is the directional wave spreading function, which satisfies $\sum_k H_{nk}(\omega_n, \theta_k)\Delta\theta = 1$. Then, NewWave in response angle is simply:

$$\phi_{NW} = \alpha_\phi \frac{\sum_n S_{\phi\phi}(\omega_n)\Delta\omega \mathrm{Re}\left[\exp(i\omega_n t)\right]}{\sum_n S_{\phi\phi}(\omega_n)\Delta\omega} \tag{10}$$

and we can define the unidirectional designer wave as the wave time history which would give the NewWave in response angle as:

$$\eta_{\phi_{NW}} = \alpha_\phi \frac{\sum_n S_{\phi\phi}(\omega_n)\Delta\omega \mathrm{Re}\left[Z_{j\theta=0}^{-1} \exp(i\omega_n t)\right]}{\sum_n S_{\phi\phi}(\omega_n)\Delta\omega} \tag{11}$$

Equivalently, the average shape of the largest waves in the incident random wave field – the NewWave in surface elevation is expressed as:

$$\eta_{NW} = \alpha_\eta \frac{\sum_n S_{\eta\eta}(\omega_n)\Delta\omega \mathrm{Re}\left[\exp(i\omega_n t)\right]}{\sum_n S_{\eta\eta}(\omega_n)\Delta\omega} \tag{12}$$

and we can define the associated response angle in time due to the NewWave in surface elevation as:

$$\phi_{\eta_{NW}} = \alpha_\eta \frac{\sum_n S_{\eta\eta}(\omega_n)\Delta\omega \mathrm{Re}\left[Z_{j\theta=0} \exp(i\omega_n t)\right]}{\sum_n S_{\eta\eta}(\omega_n)\Delta\omega} \tag{13}$$

In this analysis, we are answering two different questions.

- What is the most probably maximum hinge angle in time, and the associated input wave which produces this response?
- What is the most probable shape of extreme waves in the incident field, and the associated hinge angle motion in time?

The solutions are connected by a reciprocal relationship that will be discussed later.

4. Long-term response statistics

To provide realistic sea-state data, the Norwegian 10 km Reanalysis Archive (NORA10) hindcast data for Orkney from $1958-2011$ is used as a case study in this paper. The location of the NORA10 grid point is 58.97°N, 03.60°W. This is located $\sim$ 30 km west of the EMEC test site for marine renewable energy machines on the west coast of Orkney. From Santo et al. (2016a), it has been shown that at Orkney the mean annual wave power produced by the M4 machine is strongly correlated to the North Atlantic Oscillation (NAO), allowing the statistics of the historic mean power to be reconstructed back to 350 years, hence this location is of great interest.

The wave data available in 3 hour intervals (per sea-state) contain information such as date, time, significant wave height (H_s), peak spectral wave period (T_p), mean wave period (T_m), wind speed, wind and wave directions, and also the sea-state data split into wind sea and swell with each having H_s, T_p and wave directions provided, see Reistad et al. (2011) for more details on the NORA10 data. We first present the long-term response statistics using the entire sea-state data (defined as total sea – unimodal frequency distribution), in Section 5 we will present similar statistical analysis using the split sea data (bimodal frequency distribution). Previous analysis using the same data had compared model and buoy data in terms of the annual mean and extreme values at several locations, and in general the agreement is reasonable, see Santo et al. (2015, 2016b).

Figure 10 presents a scatter diagram of normalised occurrence of H_s and T_p for the entire 54 years of hindcast record at Orkney, with red indicating the highest number of occurrences. The two lines represent lines of constant steepness (defined as $s = H_s/T_p^2$): solid line for the constant limiting steepness ($s = 0.0576$), and dashed line for the constant mean steepness ($s = 0.0169$). The limiting steepness line in one sense represents the most severe historical sea-states ever predicted at that location during the period of the available data. This steepness also matches that presented by Socquet-Juglard et al. (2005) from a compilation of northern North Sea and Norwegian field measurements.

The standard JONSWAP spectral shape with $\gamma = 3.3$ for the peak enhancement factor is assumed for all sea-states, and the bimodal directional spreading function according to Ewans (1998) is used to model directional spread sea in fetch-limited sea-states, the proposed form is reproduced here:

$$H(f,\theta) = \frac{1}{\sqrt{8\pi}\sigma(f)} \sum_{k=-\infty}^{\infty} \left\{ \exp\left[-\frac{1}{2} \left(\frac{\theta - \theta_{m1}(f) - 2\pi k}{\sigma(f)} \right)^2 \right] + \exp\left[-\frac{1}{2} \left(\frac{\theta - \theta_{m2}(f) - 2\pi k}{\sigma(f)} \right)^2 \right] \right\} \quad (14)$$

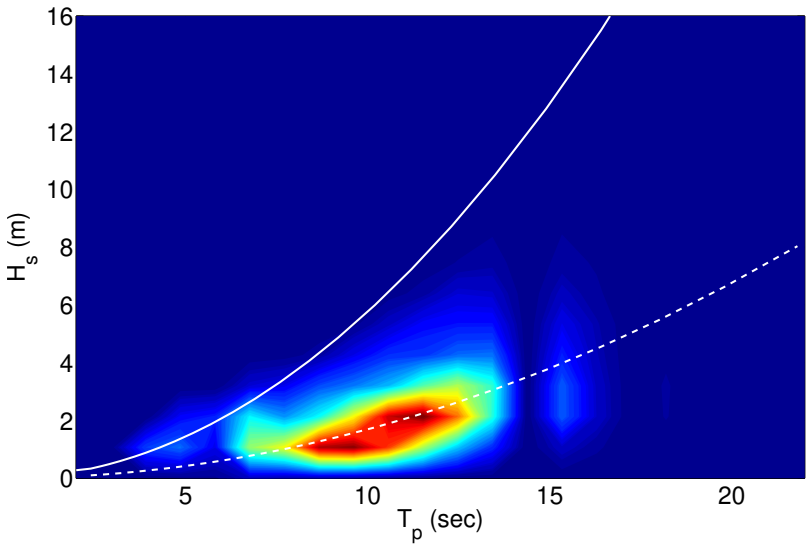

Figure 10: Scatter diagram of normalised occurrence of H_s and T_p at Orkney from $1958-2011$, with red region indicating the highest number of occurrences. Solid line represents the constant limiting steepness, dashed line represents the constant average steepness.

where $\sigma(f)$ is the angular width (a measure of the spreading of each component), and $\theta_{m1}(f)$ and $\theta_{m2}(f)$ are the locations of the peaks. The parametric forms for $\sigma(f)$ and $\theta_{m2}-\theta_{m1}$ are described in Equation 6.4 and 6.5 of Ewans (1998, p. 508). The Ewans directional distribution is unimodal for $\omega < 2\omega_p$ and splits into a bimodal form for $\omega > 2\omega_p$. Figure 11 illustrates a contour plot of the Ewans directional distribution, noting that the spectral levels at each frequency are normalised to have a maximum of one to emphasize the split of the distribution at high frequency.

The subsequent analysis initially assumes the M4 machine remains aligned along mean wave direction in both unidirectional and spread seas. Assuming deep water, the RAO is scaled up from laboratory scale to full scale, by scaling the resonant heave period of the stern float (float 3, or T_{r3}) to the long-term average wave energy period ($T_e = 8.44$ sec) at Orkney, giving a machine length of 47 m. It should be noted that the M4 machine is sized based on the long-term average T_e, by taking $T_{r3} =$ average T_e, see Santo et al. (2016a) for more details on the machine sizing.

Figure 12 shows the largest surface elevation and response in time due to Equation $10-13$ for an extreme storm of duration set to 3 hour with $H_s = 13$ m and $T_p = 15$ sec (on the limiting steepness line). The top figure shows the NewWave focussed wave group in time at the focus location without the presence of the M4 machine (η_{NW}, black line), and the associated response after the interaction

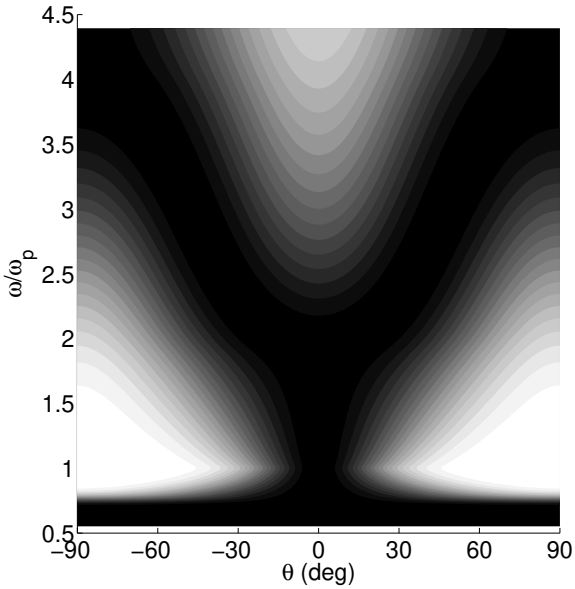

Figure 11: Contour plot of the Ewans directional distribution. Dark corresponds to high levels, light to low levels. The spectral levels at each frequency are normalised to have a maximum of one for illustration purpose.

of this wave group with the M4 machine at the 1 in 3 hour response level ($\phi_{\eta_{NW}}$, grey line). The bottom figure shows the 1 in 3 hour NewWave machine response in time (ϕ_{NW}, black line), and the associated input designer wave group that leads to the maximum expected response ($\eta_{\phi_{NW}}$, grey line). All figures are normalised by α_η. One can easily see the reciprocity in time between $\phi_{\eta_{NW}}$ and $\eta_{\phi_{NW}}$, these signals are identical in shape if one of the time axes is reversed. It can be observed that for this case, with storm T_p away from the peak period of the RAO, η_{NW} produces a small response in the machine, i.e. the machine basically rides over the crests and troughs of the long waves. On the other hand, the designer wave ($\eta_{\phi_{NW}}$) with linear crest amplitude one-third of η_{NW} but with much more appropriate wave frequency content and phasing, gives rise to the most energetic machine excitation (the expected maximum response), which is now twice as large. Hence, as far as the machine response is concerned, the designer wave is not the most extreme wave in the open ocean. Instead, it has a frequency content more matched to the M4 response, but of course of equal likelihood of the largest in 3 hours in the same sea-state. Also, it is worth noting that because the machine response is fairly narrow-banded, the wiggles in the excitation decay slowly in time (long memory effect), which is much slower than typically expected for surface elevation in

ocean, and the excitation period depends to a close approximation only on the peak frequency of the RAO, regardless of the sea-state.

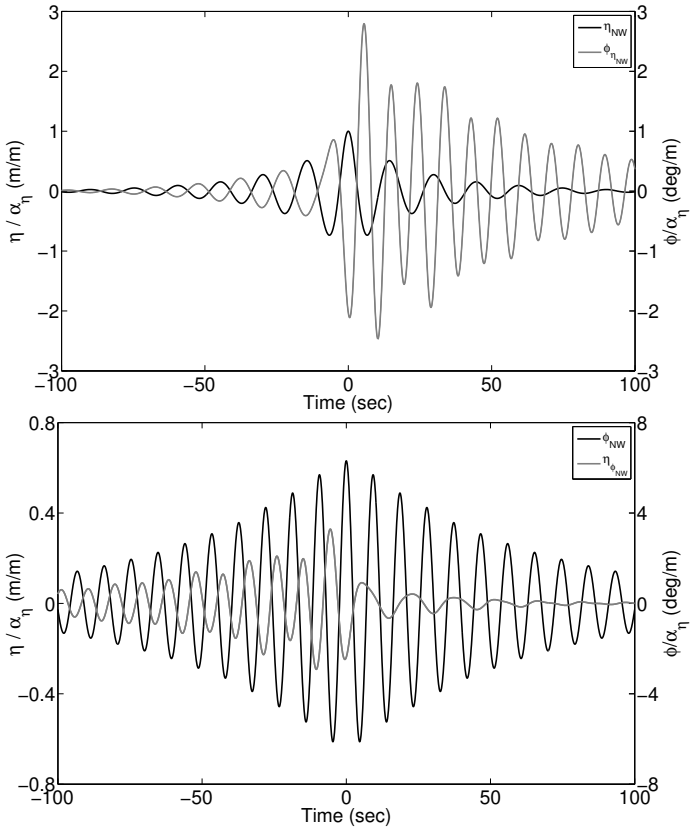

Figure 12: Top figure: Plot of the NewWave focussed wave group in time at the focus location without the presence of the M4 machine (black line), and the associated response in time due to the wave group (grey line) for 1 in 3 hour response level. Bottom figure: Plot of the NewWave machine response in time (black line), and the associated input designer wave group that leads to the maximum expected response (grey line). All plots are normalised by α_η.

Performing the NewWave in response analysis in both the limiting and mean steepness lines for the M4 machine sized for Orkney, we obtain the variation of the peak hinge angle at a 1 in 3 hour level as a function of storm T_p as shown in Figure 13. The results for unidirectional and directional sea-states are plotted in blue and red lines, respectively, and the variations along the limiting steepness and the mean steepness lines are shown in solid and dashed lines, respectively. As expected, the peak response occurs when the storm T_p is close to the peak RAO of the full scale machine (about 9.3 sec). Interestingly, as the storm T_p is further increased to represent more

severe storms (much larger waves), the machine response is close to flat (asymptotic) for constant wave steepness, demonstrating that the machine responds very similarly under the most extreme sea-states. Thus, the machine response is controlled by the steepness of the sea-state, rather than the wave height.

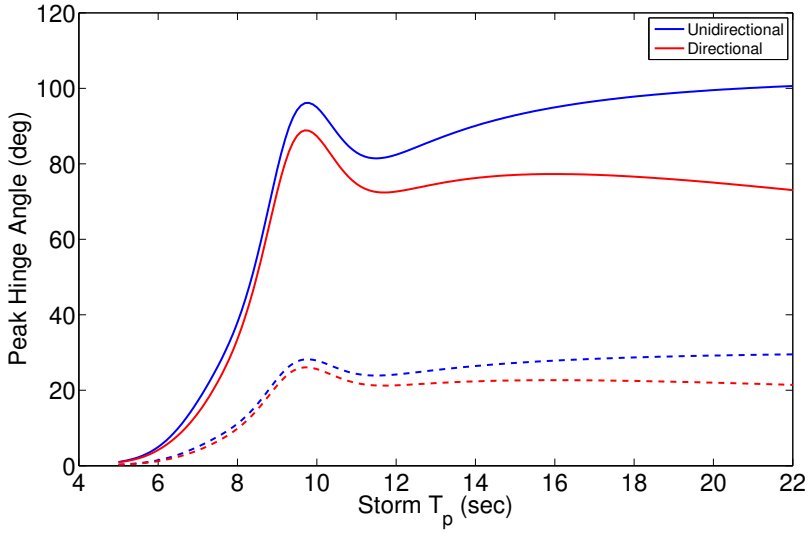

Figure 13: Peak hinge angle response for unidirectional and directional sea-states along the limiting steepness line.

The asymptotic behaviour of the machine response for large T_p is due to the behaviour of the JONSWAP high tail form (ω^{-5} tail), which is identical for any storm with the same overall steepness, see Figure 14 for an illustration. Hence, the asymptotic result along the limiting steepness case provides an upper bound for the extreme machine response. The peak responses for directional sea-states, in comparison with unidirectional sea, are reduced to about $10-20\%$ for increasing T_p due to the bimodal behaviour of Ewans spreading function at high frequency, and the reduction of the RAO with incident wave direction.

The upper bound of the extreme response is larger than 70° for both unidirectional and directional sea-state assuming linear behaviour. This peak hinge angle is clearly much too large for the present machine configuration, where $\phi \sim 40^\circ$ is the limiting angle before self-collision between float 2 and the beam connecting floats 2 and 3, a first indication that the M4 machine will not survive in the long term at Orkney. It is worth mentioning that the analysis so far neglects the effect of nonlinearity – local submergence of the floats and viscous damping for very large relative

motion, which is apparent from Figure 6. Including the effect of this nonliearity will reduce the peak response in general. Nevertheless, these linear results do give an upper bound on machine responses.

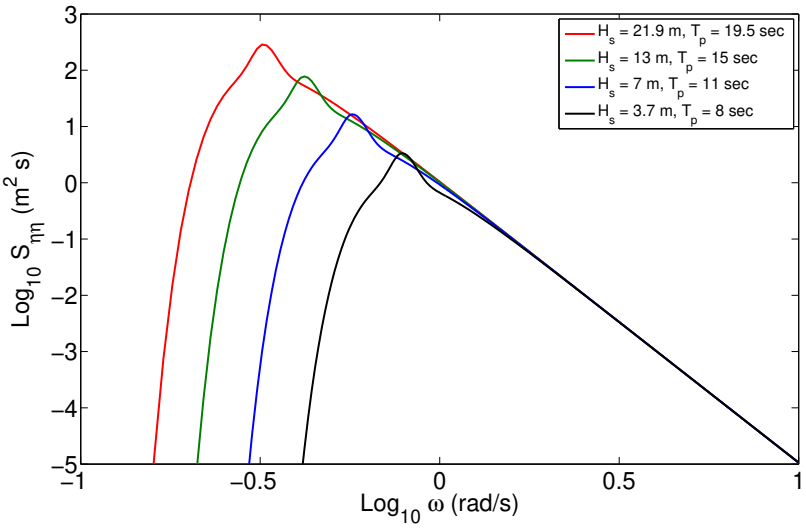

Figure 14: Universal tail form of the standard JONSWAP spectrum for all storms with same steepness (H_s/T_p^2).

Performing the extreme response analysis over 54 years of the hindcast data, we obtain the histogram of the peak hinge angle distribution over time as shown in Figure 15 for 1 in 3 hour response level for both unidirectional and directional spread sea (the first and second bar for each distribution bin). The outcomes of the long-term hinge angle response statistic are summarised in Table 1. We find a reduction in peak hinge angle when accounting for directional spreading as opposed to unidirectional, as can be seen from the histogram that for directional spread sea, the number of occurrences increases for smaller hinge angle and decreases for larger hinge angle. The reduction is represented on average by the reduction in the mean of the hinge angle distribution. However, as the extreme responses are in general much larger than the critical hinge angle, the probability of failure under these two different sea-state assumptions are of no significant difference. For directional spread sea, it is found that the machine survives 89% of the time over the entire 157791 sea-states, which is effectively the probability of the machine surviving a single randomly chosen sea-state. In other words, the average time between failure (taking this as $\phi > 40°$) is 28 hours, which is not practical for survivability.

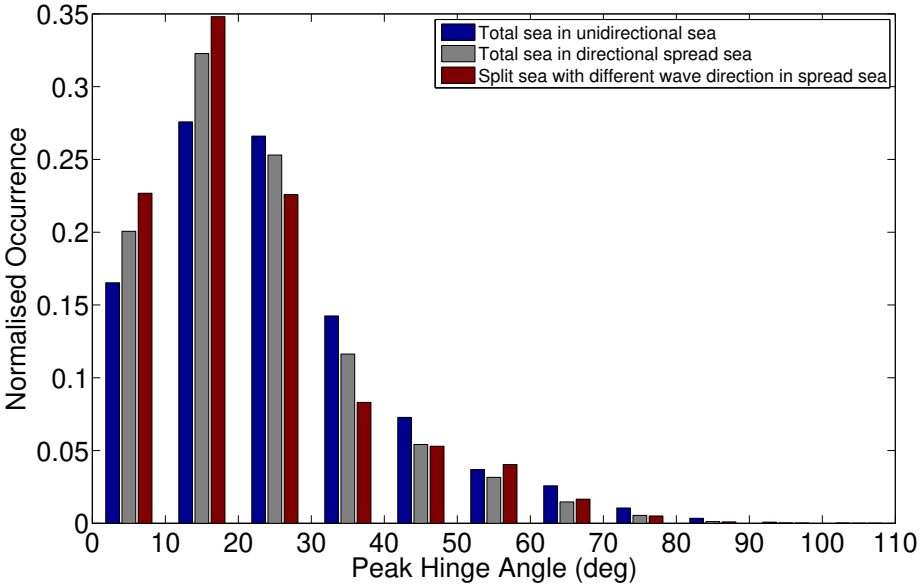

Figure 15: Histogram of the peak hinge angle distribution of the M4 machine from 1958 – 2011 at Orkney for three different sea-state assumptions. The width of the distribution bin is 10°, and each bar is placed within the bin width for clarity. The first bar on the left of each bin corresponds to unimodal frequency distribution (total sea) in unidirectional sea, the second bar corresponds to unimodal in directional spread sea, and the third bar corresponds to bimodal frequency distribution (spread sea) with different wave direction in spread sea.

5. Extreme response due to lack of alignment

The analysis so far assumes the machine is aligned along the mean wave direction in both unidirectional and spread seas, and the general finding is that there is reduction in the peak machine response when accounting for directional spreading as opposed to unidirectional. Lack of alignment of the machine could be investigated, which might further reduce the machine response. The analysis is straightforward for a unidirectional sea, with the reduction in peak hinge angle follows a similar shape as the RAO variation with incident wave direction at the peak frequency (see Figure 8). For a directionally spread sea, however, the information on the slow drift motion of the machine in yaw is apparently required, i.e. what orientation relative to the mean wave direction will the machine point to in a spread sea. The effect of yaw of the machine will be investigated in this section.

From the same NORA10 hindcast data, the total sea split into wind sea and swell are available for each sea-state, and each component contains (H_s, T_p) and peak wave direction. Hence, it is possible to include the effect of bimodality in frequency to investigate any possible reduction in

Table 1: Summary of the long-term hinge angle response statistics under four different assumptions in a randomly chosen 3 hour sea-state.

Type of sea-state assumptions	Mean of the peak hinge angle distribution	The average time between failure
Unimodal frequency distribution (total sea):		
In unidirectional sea	24.46°	20 hours
In directional spread sea	21.74°	28 hours
Bimodal frequency distribution (split sea), all in directional spread sea:		
With same mean wave direction	21.25°	25 hours
With different mean wave direction	21.06°	26 hours

extreme response by allowing for lack of machine alignment. Two additional cases are considered: bimodal frequency distribution (split sea) with the same mean wave direction, and with different mean wave direction according to each component, both cases in directional spread seas. For the latter scenario, instead of using the yaw moment (which is not available), we position the M4 machine at an arbitrary direction bounded by the peak wave direction between swell and wind sea ($\theta_{swell} - \theta_{windsea}$), and search for the direction in this range which maximizes the total motion response, and use that for long-term response statistics. This approach is conservative, because the machine is likely to wander about, so even with second order different yaw calculations, the exact approach (incident) wave direction to use remains unknown. The machine response beyond $\pm 90°$ incident wave direction relative to the machine is assumed to be insignificant, justified from the rapid roll-off of the machine RAO shown in Figure 8. The results of the response statistics for the two additional cases are shown in Table 1. The histogram of the peak hinge angle distribution for different mean wave direction is shown in Figure 15 as the third bar on each bin; the histogram for the same wave direction is not shown as both distributions are very similar.

Comparing the total sea to the split sea case, we are investigating the effect of bimodality in frequency on the extreme hinge angle response. From the histogram distribution in Figure 15, we observe some reduction in the response for $\phi < 40°$ (non-failure region), represented by an increase

in number of occurrences for $\phi < 20°$, and a decrease for $20° < \phi < 40°$. Interestingly, instead of having only response reduction when considering total sea to split sea, we also observe significant number of response enhancement for $\phi > 40°$ (failure region). Such response enhancement in split sea can go up to 60° larger than for total sea. This corresponds to the case where even though T_p for total sea is longer than the machine RAO peak period, the individual wind sea and/or swell T_p is close to the machine peak RAO period which generates a larger overall response (resonance excitation) for the split sea case than for the total sea case. As a result, the probability of machine failure increases slightly for the split sea case. Thus, the overall reduction in the response due to the effect of two peak form in frequency is only marginal, represented on average by the slight reduction in the mean of the hinge angle distribution for split sea, as compared to the total sea, all with directional spreading.

Comparing the effects of the two components (split sea) in the same mean wave direction to different direction, the response in hinge angle is reduced for the different mean direction as the wave direction between swell and wind sea ($\theta_{swell} - \theta_{windsea}$) increases. This is purely due to the effect of machine misalignment between the two dominant mean directions. Nevertheless, the largest reduction for $\phi > 40°$ (failure region) is only 13°, with most of the reduction $< 5°$, hence the overall reduction is marginal. In fact, the histograms of both cases are very similar. We further investigate whether this marginal response reduction is genuine, or an artefact due to our conservative approach by searching for the worst machine orientation. The same statistics is repeated by searching for the best machine orientation instead (which minimizes the total motion response), in which the peak of the hinge angle distribution is shifted towards 0°, however the failure region is still significant. The average time between failure increases from 26 hours for the worst machine orientation to only 36 hours for the best orientation, which is still not practical for survivability. This demonstrates that for failure criterion of $\phi > 40°$ (derived from the present machine configuration), the reduction in response for the failure region is small when considering lack of alignment of the machine. This also implies that the slow drift yaw motion of the machine is likely to have a negligible effect on survival statistics assuming predominantly linear machine.

6. Discussion and conclusions

This paper has presented a methodology for the analysis of extreme responses for the M4 wave energy converter. Although the motion of the machine is generally close to linear, we have identified

locally violent free-surface effects which seem to reduce and limit extreme motions. If any of the floats is overtopped, then there will be a local loss of hydrostatic stiffness and a considerable amount of associated dissipation of energy. It is difficult to include such localised effects into a spectral model, so this is left for future work.

What this paper does present are upper estimates of the M4 response in violent sea-states where survival of the machine is in question. Very large angular displacements of the hinge could be designed for relatively easily, by replacing the straight beam between floats 2 and 3 by one with a 'dog-leg' shape. If the M4 design can be modified to survive at the open North Atlantic west of Orkney, it is likely to survive almost everywhere.

To summarise, we find that:

- the machine response is remarkably linear, even for large motions of 30° in hinge angle, with weak nonlinearity in bending moment,
- during the excitation phase driven by the main wave group, there is locally complex and violent free-surface effects which generally reduce the overall machine motions,
- during the free-vibration phase after the main group has moved away from the machine motion, the decaying machine response can be characterised by simple linear radiation damping,
- with Orkney as a case study using NORA10 hindcast data, we observe that the machine response is controlled by the steepness of sea-states, with asymptotic response for storm T_p longer than the peak RAO period of the full scale machine,
- long-term linear response statistics over the hindcast data period, with critical hinge angle $\phi > 40°$, estimates that the machine fails at Orkney once every 28 hours on average,
- there is a reduction in the extreme response of the machine when accounting for directional spreading, however the reduction is only marginal when accounting for bimodality in frequency (from total sea to split sea) in spread seas,
- the effect of machine misalignment on the extreme response reduction is small in split sea, hence the effect of slow drift yaw motion of the machine appears to be an unimportant parameter for survivability,

- this linear analysis provides an upper bound of the extreme response, which can be accounted for in the design relatively easily.

This paper has presented a combination of experimental, numerical and analytical studies, followed by long-term linear response statistics for extreme motions of the M4 machine for survivability. It is worth emphasizing that the study presented is not only relevant to the M4 machine, but because of the implications, the methodology approach used here is potentially relevant to other wave energy converters as well.

Acknowledgements

We thank Dr. Richard Gibson now at Offshore Consulting Group and BP Sunbury for providing the wave data and acknowledge support from EPSRC (project EP/J010316/1 Supergen MARine TechnologY challenge and project EP/K012487/1 Supergen Marine Challenge 2 Step-WEC).

References

Ambühl, S., Sterndorff, M., Sørensen, J. D., 2014. Extrapolation of extreme response for different mooring line systems of floating wave energy converters. International Journal of Marine Energy 7, 1–19.

Boccotti, P., 1983. Some new results on statistical properties of wind waves. Applied Ocean Research 5 (3), 134–140.

Eatock Taylor, R., Chau, F., 1992. Wave diffraction theorysome developments in linear and non-linear theory. Journal of Offshore Mechanics and Arctic Engineering 114 (3), 185–194.

Eatock Taylor, R., Taylor, P. H., Stansby, P. K., 2016. A coupled hydrodynamic-structural model of the M4 wave energy converter. Journal of Fluids and Structures 63, 77–96.

Ewans, K. C., 1998. Observations of the directional spectrum of fetch-limited waves. Journal of Physical Oceanography 28 (3), 495–512.

Grice, J., Taylor, P., Taylor, R. E., 2013. Near-trapping effects for multi-column structures in deterministic and random waves. Ocean Engineering 58, 60–77.

Jonathan, P., Taylor, P. H., 1997. On irregular, nonlinear waves in a spread sea. Journal of Offshore Mechanics and Arctic Engineering 119, 37.

Lindgren, G., 1970. Some properties of a normal process near a local maximum. The Annals of Mathematical Statistics, 1870–1883.

Muliawan, M. J., Gao, Z., Moan, T., 2013a. Application of the contour line method for estimating extreme responses in the mooring lines of a two-body floating wave energy converter. Journal of Offshore Mechanics and Arctic Engineering 135 (3), 031301.

Muliawan, M. J., Karimirad, M., Gao, Z., Moan, T., 2013b. Extreme responses of a combined spar-type floating wind turbine and floating wave energy converter (STC) system with survival modes. Ocean Engineering 65, 71–82.

Newland, D. E., 2006. Mechanical Vibration Analysis and Computation. Courier Corporation.

Parmeggiani, S., Kofoed, J. P., Friis-Madsen, E., 2011. Extreme loads on the mooring lines and survivability mode for the wave dragon wave energy converter. In: World Renewable Energy Congress 2011.

Reistad, M., Breivik, Ø., Haakenstad, H., Aarnes, O. J., Furevik, B. R., Bidlot, J.-R., 2011. A high-resolution hindcast of wind and waves for the North Sea, the Norwegian Sea, and the Barents Sea. Journal of Geophysical Research: Oceans (1978–2012) 116 (C5).

Santo, H., Taylor, P., Eatock Taylor, R., Stansby, P., 2016a. Decadal variability of wave power production in the North-East Atlantic and North Sea for the M4 machine. Renewable Energy 91, 442–450.

Santo, H., Taylor, P. H., Eatock Taylor, R., Choo, Y. S., 2013. Average properties of the largest waves in Hurricane Camille. Journal of Offshore Mechanics and Arctic Engineering 135, 011602.

Santo, H., Taylor, P. H., Gibson, R., 2016b. Decadal variability of extreme wave heights as a measure of storm severity in the North-East Atlantic and North Sea. In preparation.

Santo, H., Taylor, P. H., Woollings, T., Poulson, S., 2015. Decadal wave power variability in the North-East Atlantic and North Sea. Geophysical Research Letters 42 (12), 4956–4963.

Socquet-Juglard, H., Dysthe, K., Trulsen, K., Krogstad, H. E., Liu, J., 2005. Probability distributions of surface gravity waves during spectral changes. Journal of Fluid Mechanics 542, 195–216.

Stansby, P., Moreno, E. C., Stallard, T., 2015a. Capture width of the three-float multi-mode multi-resonance broadband wave energy line absorber M4 from laboratory studies with irregular waves of different spectral shape and directional spread. Journal of Ocean Engineering and Marine Energy, 1–12.

Stansby, P., Moreno, E. C., Stallard, T., Maggi, A., 2015b. Three-float broad-band resonant line absorber with surge for wave energy conversion. Renewable Energy 78, 132–140.

Sun, L., Eatock Taylor, R., Taylor, P., 2015. Wave driven free surface motion in the gap between a tanker and an FLNG barge. Applied Ocean Research 51, 331–349.

Tromans, P. S., Anaturk, A. R., Hagemeijer, P., 1991. A new model for the kinematics of large ocean waves. In: Proceedings of the International Society of Offshore and Polar Engineering Conference (ISOPE-91).

Walker, D. A. G., Taylor, P. H., Eatock Taylor, R., 2005. The shape of large surface waves on the open sea and the Draupner New Year wave. Applied Ocean Research 26 (3), 73–83.

Wolgamot, H., Taylor, P., Taylor, R. E., van den Bremer, T., Raby, A., Whittaker, C., 2016. Experimental observation of a near-motion-trapped mode: free motion in heave with negligible radiation. Journal of Fluid Mechanics 786, R5.